Prediction of Feasibility of Polaronic OER on (110) Surface of Rutile TiO$_2$

Hori Pada Sarker[1,2,3]*, Frank Abild-Pedersen*[1,3,] and *Michal Bajdich*[1,3]*

[1]*Liquid Sunlight Alliance (LiSA)*
California Institute of Technology, Pasadena, CA 91125, USA

[2]*Department of Chemical Engineering, Stanford University*
443 Via Ortega, Stanford, CA 94305, USA

[3]*SUNCAT Center for Interface Science and Catalysis*
SLAC National Accelerator Laboratory
2575 Sand Hill Road, Menlo Park, CA 94025, USA

[*]Corresponding e-mail address: bajdich@slac.stanford.edu

ABSTRACT

The polaronic effects at the atomic level hold paramount significance for advancing the efficacy of transition metal oxides in applications pertinent to renewable energy. The lattice-distortion localization of photoexcited carriers in the form of polarons plays a pivotal role in the photocatalysis. This investigation focuses on rutile TiO$_2$, an important material extensively explored for solar energy conversion in artificial photosynthesis, specifically targeting the generation of green H$_2$ through photoelectrochemical (PEC) H$_2$O splitting. By employing Hubbard-U corrected and hybrid density functional theory (DFT) methods, we systematically probe the polaronic effects in the catalysis of oxygen evolution reaction (OER) on the (110) surface of rutile TiO$_2$. Theoretical understanding of polarons within the surface, coupled with simulations of OER at distinct titanium (Ti) and oxygen (O) active sites, reveals diverse polaron formation energies within the lattice sites with strong preference for bulk and surface bridge oxygen (O$_b$) sites. Moreover, we provide the evidence for the facilitative role of polarons in mitigating OER. We find that hole polarons situated at the equatorial positions near the Ti - active site, along with bridge hole polarons distal from the O$_b$ active site yield a reduction in OER overpotential by (4.6-6.5)%. We also find that having hole polarons stabilize the *OH, *O, and *OOH intermediate species when compared to case without hole polarons. This study unravels a detailed mechanistic insights into polaron-mediated OER, offering a promising avenue for augmenting the catalytic prowess of transition metal oxide-based photocatalysts catering to renewable energy requisites.

Key words: Solar fuel, Hydrogen, Rutile TiO$_2$, Polaron, Density Functional Theory (DFT)

INTRODUCTION

Capturing solar photons and converting them into chemical energy, such as fuels, represents one of the promising pathways to mitigate environmental and climate catastrophes, achieve energy

1

security and independence, and establish a sustainable global economy, as demonstrated by numerous studies[1–5]. This is the underlying reason why researchers worldwide are actively working on the advancement of solar-driven fuel generation technologies. These endeavors include artificial photosynthesis aimed at producing environmentally friendly hydrogen (H_2) and solar-driven reduction of CO_2 into energy-dense fuels such as ethanol[6–8]. At the core of these solar-driven technologies, photoactive semiconducting materials play a crucial role in capturing solar photons and storing their energy within the chemical bonds of such fuels. Among the multitude of available photo-absorber materials, photo-active transition metal oxides (TMOs) stand out for their exceptional solar energy harvesting capabilities. With over 200 suitable photo-active TMO options, these materials have demonstrated potential for solar energy harvesting[9,10].

Among all TMO's, TiO_2 is one of the most studied photoanode materials for PEC water splitting[11]. TiO_2 has become a benchmarked material for understanding PEC water splitting due to its photo response within the UV and some part of the visible spectrum, high crystallinity, stability in aqueous solution, resistant to (photo) corrosion, non-toxicity, abundance and low cost[12,13]. Despite being one of the most widely studied photo-active materials, TiO_2 has major drawbacks in terms of UV-adsorption spectrum, carrier transport, particularly for efficient extraction and utilization of photogenerated charge carriers which eventually contribute to the higher overpotential associated with OER[14]. In fact, carrier transport limitation phenomenon is prevalent almost all the TMO based photocatalysts[15,16]. Poor carrier separation, carrier recombination, and slow carrier transfer kinetics are considered as the major efficiency loss channels among others.

In TiO_2 as well as other TMO's, slow moving carriers induce strong carrier-lattice interaction and subsequently distorts the lattice locally. Such a local distortion in lattice forms an attractive potential within which slow moving carriers get trapped and form localized polarons. Formation of polarons in TiO_2 as well as other TMO's are well established both experimentally[17–22] and theoretically[23–32]. The review paper by Cesare Franchini et. al.[28] provided a list of polaron forming materials along with the characterization techniques employed in these studies. Photoexcitation induced polaron formation, dynamic nanoscale lattice distortion as well as associated strain field, all are central aspects of photocatalysis, and play a crucial role in photocatalytic chemical reactions[33]. However, the role of photoexcited polarons in photocatalysis is quite unclear and not well studied.

2

In light of this, we studied hole polarons on a prototypical rutile TiO_2 (110) model surface using first principles density functional theory to understand whether it has any effects on OER catalytic activity. In a recent study, Patrick Gono et. al.[27] reported a slight reduction of OER overpotential on the rutile TiO_2 (110) surface. They concluded that the OER overpotential reduction happens due to the presence of surface hole polaron. Inspired by this study, we conducted a thorough study to address in particular the differences between the polaronic and non-polaronic OER mechanism, what types of polarons sites exists and what is their overall effect on OER overpotential. We address the above questions by estimating polaronic stability, calculating polaronic electronic structure, the OER free energy landscape as well as the OER catalytic activity in terms of an OER volcano plot. We shall explain the concept in detail later. The OER on TiO_2 surface is a well-established chemical process, with numerous studies documented in the scientific literature[12,26,27,34].

Despite this, there is a scarcity of research that examines the mechanism of OER on the TiO_2 surface when there is polaron. In fact, there are very few studies on photoexcited polaronic effects in photo-driven catalysis. Cheng Cheng et. al.[35] reported enhanced electron polaron photoactivity in rutile TiO_2 (110) surface upon CO adsorption during CO_2RR. They demonstrated that CO adsorption drives subsurface electron polarons towards the surface-active sites, thus makes them chemically photoactive. Burak Guzelturk et. al.[36] reported that local distortion/phonon cloud associated with the polarons enhances the carrier mobility in photovoltaic lead halide perovskites by protecting them from scattering off from defect centers. Contrary, Lohaus et.al.[37] in their hematite (α-Fe_2O_3) paper postulated a polaron induced photovoltage limitation by Fermi level pinning, hence PEC water splitting efficiency limitation, by measuring quasi-Fermi level splitting. Julia Wiktor et. al.[38] demonstrated that polaronic levels affect the alignment at the solid-liquid interface and the carrier recombination happens via polarons in the PEC water splitting reaction. Rettie et. al. found a significant reduction of carrier mobility in W: $BiVO_4$ by polaron. So, in light of this, it becomes highly crucial to gain a more profound understanding at the atomic level regarding the OER mechanism involving polarons. In addition, exploring any potential connections between photoexcited polarons and the photocatalytic performance become important. This knowledge is essential not only to address the efficiency limitations but also to formulate a cost-effective approach and propose efficient photocatalytic materials aimed at producing sustainable and renewable solar fuels.

In this study, we present a detailed characterization of polaron formation using Hubbard-U-corrected and hybrid density functional theory (DFT) calculations. We investigate polaron formation probability via thermodynamic free energy calculations at various positions within the bulk and on the surface of TiO_2, as well as the band-alignment energetics of polaronic states within the band gap. Additionally, we analyze the full free energy landscape of OER as well as compare the catalytic activity with and without the presence of hole polarons. Finally, we discuss our calculated data in context of available experimental results.

COMPUTATIONAL METHODS

We performed spin polarized density functional theory (DFT) calculations using the Vienna ab initio Simulation Package (VASP - 5.4.4)[40] within the python-based atomic simulation environment (ASE)[41]. The exchange and correlations were described by Perdew-Burke-Ernzerhof (PBE) functional within the generalized gradient approximation (GGA)[42] and hybrid and Hubbard-U corrections were applied as discussed below . Projector-augmented plane wave (PAW)[43] method with a kinetic energy cut-off of 500 eV was used to treat the ion-electron interaction throughout all calculations, which gave well converged results. Our approach involved utilizing TiO_2 (110) surfaces, a (2×2) 4 - layers surface containing 96 atoms, (2×2) 6 – layers containing 144 atoms, and (4×2) 4 - layers surface containing 192 atoms, to model hole polaron and simulate OER at Ti_{cus} (coordinatively unsaturated Ti - site) and O_b (bridge O - site) active sites, respectively. For all surface calculations, at least 20 Å vacuum was employed between the repeating slabs in order to avoid spurious image-charge interactions. The bottom two layers were kept fixed to bulk geometry and top two layers as well as adsorbates (*OH, *O, and *OOH) were allowed to relax in all directions during surface geometry optimization bellow the force threshold of 0.02 eV Å^{-1}. The k-point mesh was sampled using the Mohkhorst-Pack scheme. A 7×3×1 k-point grid was employed for geometry optimization and polaron localization in (2×2) 4-layers and (2×2) 6-layers surfaces. For the (4×2) 4 -layers surface, a 3×3×1 k-point grid was utilized. To model hole polaron, we introduce an additional hole to the relaxed surface. Along with adding the extra hole, we initially introduced a small perturbation around the site of the polaron to break the local lattice symmetry before proceeding structural relaxation. Furthermore, to maintain charge neutrality of the surface, we incorporated a compensating homogeneous background counter charge as implemented by VASP. Polaron binding energy was calculated using the following formula[23]-

$$E_{bind}^{\pm} = E^{polaron}(N \mp 1) - E^{perf}(N \mp 1), \qquad (1)$$

where $E_{bind}^{\pm}$ is the polaron binding energy and (+) sign corresponds to hole polaron, while (-) sign corresponds to electron polaron. A negative $E_{bind}^{\pm}$ implies energy gain and hence formation of a stable polaron. $E^{polaron}$ and E^{perf} are the total DFT energies of the system with extra charge in polaronic (distorted geometry) and non-polaronic (undistorted) geometry, respectively. The number of electrons is given in parenthesis, where N represents total number of electrons of the neutral system.

DFT is known to underestimate electron self-interaction corrections (SIC)[44–46]. Due to the SIC errors, DFT often fails to produce a desired localized polaronic solution. Hybrid density functional as well as Hubbard U correction can overcome the SIC error. To address the charge delocalization issue present in the standard DFT method, we implemented a Hubbard-U correction targeting the atoms where polarons are localized. We also employed hybrid density functional (HSE06)[47] method to benchmark the U value applied in this study (**Figure S1**). An effective U value (U_{eff}) of 10 eV to O 2p-orbital at polaronic site was employed [25,29,30,48]. The specific O-atom were the stabilized hole polaron was chosen as by Deskin and Dupuis et. al.[30] Using U_{eff} of 10 eV, they successfully localized hole polaron at O-site and estimated hole mobility which is in good agreement with experiment. In $BiVO_4$, Pasumarthi et. al.[49] and Liu et. al.[50] also applied an U_{eff} value of 9 eV to localize hole polaron at a single oxygen atom. Liu et. al. showed that $U_{eff} = 9$ eV satisfied the behavior of piece-linearity of DFT energies with respect to fractional occupation.

For electron localization at Ti^{+3}-site in reduced rutile TiO_2, many studies applied U_{eff} values ranging from (3.3-5.5)eV[17,24,29,48,51]. For example, Deskin et. al.[29] applied an U_{eff} value of 4.1eV to localize electron polaron at Ti-site in rutile TiO_2. Stevin et. al.[17] applied an U_{eff} value of 3.9eV to generate stable electron polaron on defect free rutile TiO_2 (110) surface. Selcuk and Selloni et. al.[24] also applied a similar value of $U_{eff} = 3.9$ eV to localize electron polaron on anatase (101) and (001) surface. Carmen J. Calzado et. al.[51] applied an $U_{eff} = 5.5$ eV to localize electron polaron on reduced rutile TiO_2 surface and demonstrated that the electron polaronic state is located ~1 eV below the conduction band edge which is reported in many published literatures[26,52]. Similar to Carmen J. Calzado et. al.[51], we applied an $U_{eff} = 5.5$ eV to Ti 3d orbitals to localize electron polaron on reduced rutile TiO_2 surface in this study. Moreover, the applied U_{eff} values in this study successfully reproduced our hybrid DFT calculated magnetic moment ($\sim 0.75\ \mu_B$ for electron and

~ 0.68 μ_B for hole polaron), as well as hole polaronic state within band gap, for TiO$_2$ bulk (**Figure S2**).

RESULTS AND DISCUSSIONS

Hole polaron in the bulk of rutile TiO$_2$

In this study, we considered rutile phase of TiO$_2$ [tetragonal; P4$_2$/mnm; a = b = 4.66Å (exp[53]=4.58Å), c = 2.97Å (exp[53]=2.95Å)] and its (110) surface was derived from the optimized unit cell according the Computational Methods section and SI **Figure S3**.
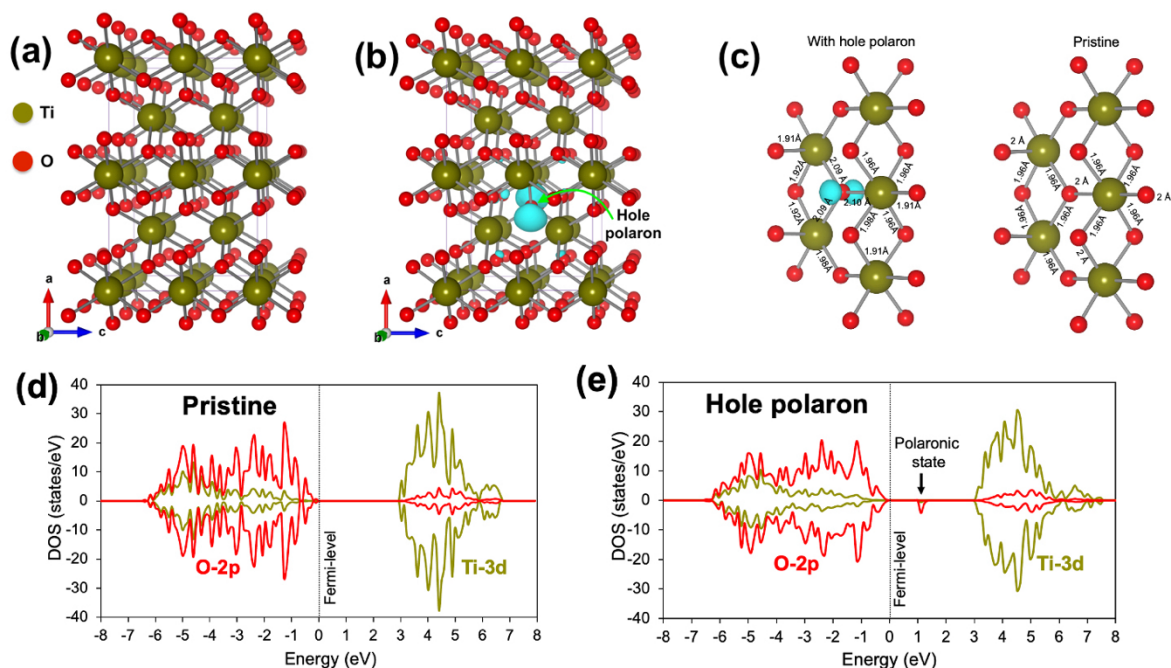
***Figure 1**. Fully DFT optimized ball and stick structural models of (a) TiO$_2$ bulk crystal structure and (b) bulk hole polaron at O-site. The iso-surfaces (azure blue color) indicate the hole polaron at oxygen site at value of 0.005 eÅ^{-3}. (c) Comparison of the local distortion with and without hole polaron. (d) Density of states (DOS) for pristine bulk and (e) for bulk hole polaron. For both case, DOS are calculated using hybrid density functional level of DFT (HSE06).*

Figure 1a shows the optimized bulk while **Figure S3** shows the corresponding (110) surface geometry. TiO$_2$ (110) surface has two distinct type of Ti atoms. They are five coordinated Ti$_{cus}$ (coordinatively unsaturated) and six coordinated Ti$_{css}$ (coordinatively saturated) sites. Like Ti – atoms, oxygen atoms also have two distinctive classifications, and they are two coordinated bridge oxygen (O$_b$) and three coordinated planner oxygen (O$_p$), and hole polarons form at O –

6

atoms in rutile TiO_2. In fact, in strongly correlated systems i.e., TiO_2 as well as other TMO's[28], polaron formation is an ubiquitous phenomenon. Due to strong carrier-lattice interaction, photoexcited or defect generated charge carriers interact and couple with optical phonons, and hence form polaron. It is well established experimentally[18,20,21,54] and theoretically[17,23,28–32] that TiO_2 forms polaron. An electron polaron forms at Ti – sites and a hole polaron at O – sites. The rationale behind the site selectivity of polaron formation in TiO_2 is that the valence band (VB) is predominantly composed of O - 2p orbitals and conduction band (CB) primarily has Ti - 3d character as shown in the density of states (DOS) plot (see **Figure1d**). So, when charge carriers are generated through photoexcitation or defect formation, they localize as hole polarons in the valence band, occupying O 2p states, and as electron polarons in the conduction band, filling up empty Ti 3d states. **Figure 1(b)** shows the iso-surface charge density of a hole polaron in TiO_2 bulk. It is obvious from the shape of the orbital shown in Figure 1b that the hole polaron occupies O $2p_z$ orbitals. It is also evident from local lattice distortion around the polaronic site (**Figure 1c**) and magnetic moment of that specific site (**Figure S4**) that hole polaron forms at O-site. Due to hole localization as polaron, Ti – O bonds around the polaronic site become distorted by $\sim$ (2-8)% compared to equilibrium Ti - O bond length (**Figure 1c**) which generates a local magnetic moment of approximately $0.68\ \mu_B$ for hole polaronic site (see **Figure S4**), within TiO_2 bulk. As a consequence of polaron formation, that particular O site changed its oxidation state from $O^{2-} \rightarrow O^-$ for hole polaron.

Surface hole polaron geometry, stability, and energy levels

We now turn our discussion to surface hole polaron on rutile TiO_2 (110) clean surface. We have stabilized hole polarons separately in five different O sites; categorized as bulk, subsurface, axial, equatorial, and bridge hole polaron (see **Figure 2a**). From the iso-surface charge density, it is evident that hole polarons occupy the O ($2p_z$) orbital. Hole polaron localization also change the local bonding environment and create local distortion around the particular polaronic site. The local Ti – O bond length near the polaronic site changes approximately (2-8)% compared to the equilibrium Ti – O bond length of an undistorted (pristine) geometry. The local bond length

7
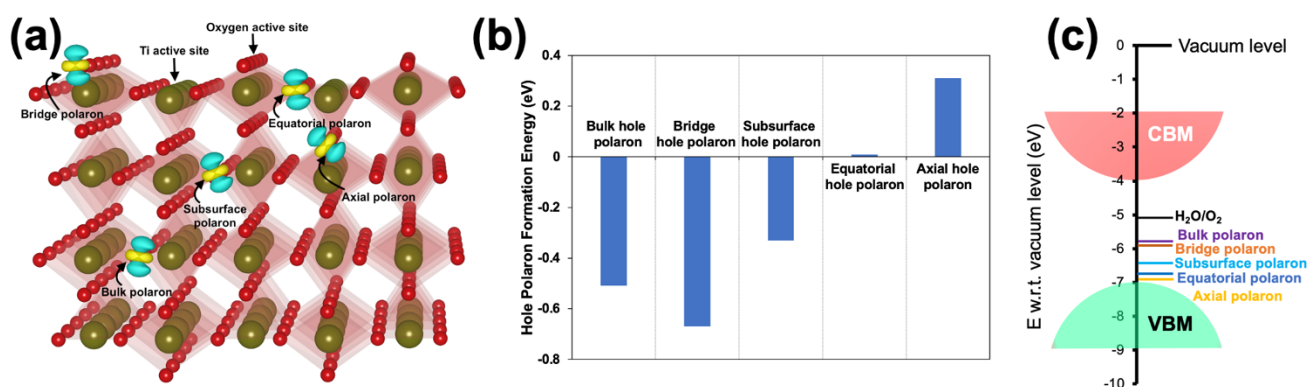
Figure 2. *(a) Schematic diagram of different hole polaron configurations on (110) surface similar to Figure 1. (b) Thermodynamics of hole polaron formation energies at different configurations as shown in (a).(c) Schematic diagram of polaronic energy level for different hole polaron configurations with respect to band edges of TiO_2. The water redox potential (H_2O/O_2) is indicated as black solid line relative to vacuum at -4.6 eV.*

change happens due to weakening of Ti (3d) – O (2p) orbital hybridization. The detail of Ti – O bond length change due to hole polaron formation at different polaronic configurations is demonstrated in **Figure S6**. Moreover, hole polaron formation also changes the oxidation state of that particular O site from $O^{2-} \rightarrow O^{-}$. It is known that the catalytic activity gets influenced by changes in the local environment, including oxidation state and bond length[33]. Clearly, the simultaneous variation in oxidation state and Ti– O bond length in the vicinity of active site will significantly impact the kinetics of the OER reaction, a topic that will be discussed in a later section. **Figure 2(b)** shows the thermodynamic stability of a polaron at different configurations of TiO_2 (110) surface, where we used equation (1) to estimate the thermodynamic stability of the polaron. As described in the Computational Methods section, a negative formation energy represent a stable (exothermic) defect. We have referenced the bulk hole polaron formation energy to a configuration where hole polaron is deep inside the surface. The hole polaron formation energy in TiO_2 bulk is $-0.56\ eV$. On the other hand, we have calculated the hole polaron formation energy (from total DFT energies) for subsurface, axial, equatorial, and bridge O site polarons are $-0.33\ eV$, $0.31\ eV$, $0.01\ eV$, and $-0.67\ eV$, respectively. Clearly, bulk and bridge site hole polarons are thermodynamically the most stable. The subsurface (2nd layer) position is also the 2nd most stable polaron configuration followed by equatorial positions and then by the axial position as the least stable one among the configurations considered. Even though, these energies

8

https://doi.org/10.26434/chemrxiv-2023-cm4p3 **ORCID:** https://orcid.org/0000-0001-9162-537X Content not peer-reviewed by ChemRxiv. **License:** CC BY-NC-ND 4.0

are derived from a purely static point (no applied potential or configuration entropy is involved) of view, they can yield some insights into the polaron defect population in a surface in a dynamic situation. Since equilibrium defect concentration (c) at temperature T follows Boltzmann distribution as [55,56].

$$c = N \, exp^{\left(-\frac{\Delta G_f}{K_B T}\right)}, \qquad (2)$$

where N represents the number of associated atomic sites, ΔG_f is estimated energy for formation of a hole polaron (see **Figure 2b**), and K_B Boltzmann's constant it is evident that hole polarons are most likely to form at the bridge sites on the surface followed by the bulk atomic sites. There is less chance for hole polarons forming at subsurface position by ~ four orders of magnitude at room temperature. The chances of forming hole polaron in equatorial and axial position are even lower. Additionally, the bridge hole polarons are clearly thermodynamically more stable than hole polarons that are beneath the surface, suggesting preference of polaron hopping towards the surface given enough energy from thermal excitations.

Such behavior contrasts with the type of conduction seen in non-polaronic semiconductors like silicon (Si), where conduction occurs through band type conduction. For rutile TiO_2, it was demonstrated by Deskin et al.[30] that hole polarons have significant ~ 0.5 – 0.62 eV site to site hoping barrier. Cheng Cheng et al[35]. showed that when CO is adsorbed on the active sites of the surface, electron polarons located in the bulk or subsurface can hop to active surface sites through a thermally driven site to site hopping mechanism. It is important to note that our study did not involve any transport or barrier calculations of polarons. Instead, we focused on assessing changes in free energy at each step of the OER process as discussed next.

So far, we have discussed hole polaronic geometries and their thermodynamic stability. Now, we will discuss the relative position of polaronic states since they play crucial role in photocatalysis, optoelectronic and other photo-driven applications. In general, the electronic structure of metal oxides relies on crystal symmetry, metal – oxygen bonding, and atomic orbital hybridization. An ideal crystal consists of filled valence band and unoccupied conduction band separated by a bandgap specific to the metal oxides. However, the presence of defects, like charge or point defects alters crystal symmetry, metal-oxygen bonding, and orbital hybridization. As a consequence, these defects in metal oxides create new electronic states within the bandgap. Like

point defects, a polaron also generates an energy level within the bandgap. The relative position of polaronic energy level with respect to the band-edges depends on the degree of charge localization and local lattice distortion. In this work, we estimated the relative position of hole polaronic energy levels of bulk as well as surface hole polarons in rutile TiO_2 **(Figure-2c)**. The estimated position of the bulk hole polaronic energy level is approximately 1.1 eV above the valence band maximum (VBM). Through a nonempirical and self-consistent optimization of Hartree-Fock exchange, A. R. Elmaslmane et. al.[57] also estimated the charge transition level (CTL) of bulk hole polaron at (1.18-1.23) eV above VBM in anatase TiO_2. We also estimated surface polaronic energy level of hole polarons at different position in rutile TiO_2 (110) surface. shows the relative position of hole polaronic states calculated with respect to the common vacuum energy level[58] (For detail, see **Figure-S7**).

Among all the hole polarons considered for (110) surface, the axial hole polaron generated a shallow defect level relative to valence band edge ($\Delta E \approx 0$). Here, ΔE is the energy difference between polaronic state and valence band edge which determines how easily a defect level can be ionized. Equatorial hole polaronic level is located near to VBM ($\Delta E \approx 0.2$ eV). Unlike axial and equatorial hole polaron, subsurface and bridge hole polaron generate deep defect levels within the band gap. For subsurface and bridge hole polaron, ΔE is approximately 0.5 eV and 0.95 eV, respectively. Therefore, the axial hole polarons will be easily ionized via thermal excitations at room temperature, while bulk, subsurface, and bridge hole polarons will be more difficult to ionize. However, surface, solvent and thermal effects may improve the utility of such deep lying polarons. Moreover, they might act as a recombination center for minority carrier, in this case, electrons. As shown in **Figure 2(c)**, even though the hole polaron energy levels are far below with respect to water redox potential (H_2O/O_2), they (except axial and equatorial hole polaron) might not be driven to OER active - sites due to the localized and deep nature of associated polaronic energy level.

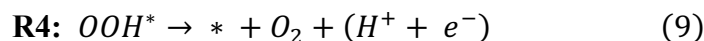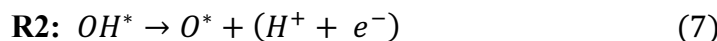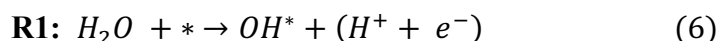**OER mechanism with polaron on rutile TiO_2 (110) surface**

The overall PEC water splitting reaction can be written as

$$2H_2O(l) \rightarrow 2H_2(g) + O_2(g). \qquad (3)$$
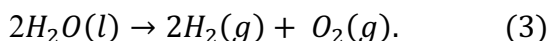
The two half reactions: water oxidation (oxygen evolution reaction, OER) and reduction (hydrogen evolution reaction, HER) that occur at the anode and cathode, respectively, and can be expressed as follows:

Acidic OER: $2H_2O \rightarrow O_2 + 4(H^+ + e^-)$ (4)

Acidic HER: $4H^+ + 4e^- \rightarrow 2H_2$ (5)
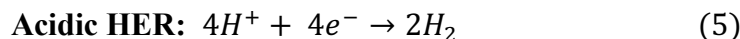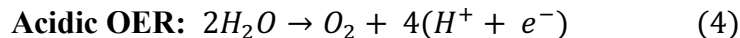
Based on equation (4), OER is a four protons coupled four electrons transfer (PCET) process, and each PCET requires at least 1.23 eV energy under standard equilibrium conditions. Therefore, the complete OER requires at least 4.92 eV (i.e., 4 × 1.23 eV) minimum energy to split two H_2O molecules into one O_2 molecule. The overall acidic OER single site mechanism can be divided into four separate steps[14].

R1: $H_2O + * \rightarrow OH^* + (H^+ + e^-)$ (6)

R2: $OH^* \rightarrow O^* + (H^+ + e^-)$ (7)

R3: $O^* + H_2O \rightarrow OOH^* + (H^+ + e^-)$ (8)

R4: $OOH^* \rightarrow * + O_2 + (H^+ + e^-)$ (9)

Where * represents an empty active site and X* represents adsorbate X at the active site. We calculate the associated Gibbs free energy change for every reaction involving intermediate adsorbates i.e., OH*, O*, and OOH* using previously developed method[14,59].
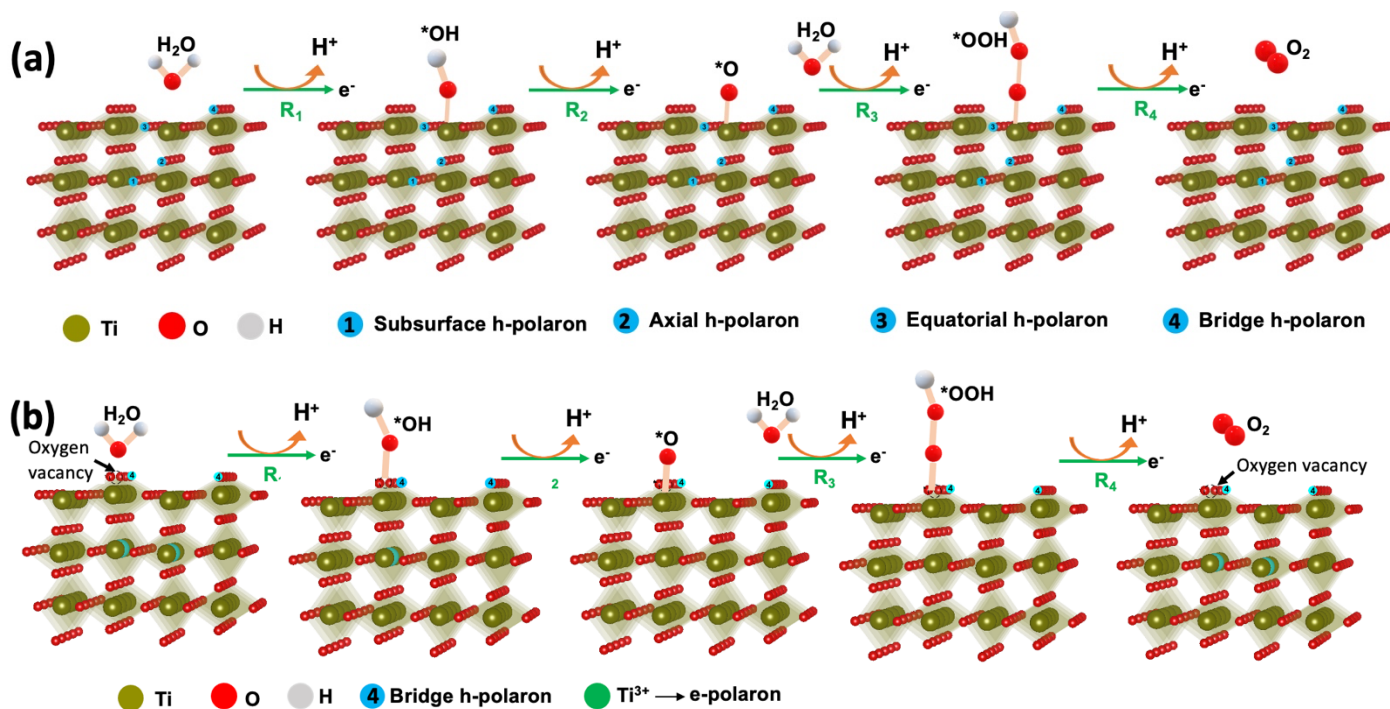
$$\Delta G_{R1} = \Delta G_{HO*} - \Delta G_{H_2O(l)} - eU + K_B T \, ln(10) \, pH \qquad (10)$$

$$\Delta G_{R2} = \Delta G_{O*} - \Delta G_{HO*} - eU + K_B T \, ln(10) \, pH \qquad (11)$$

$$\Delta G_{R3} = \Delta G_{HOO*} - \Delta G_{O*} - eU + K_B T \, ln(10) \, pH \qquad (12)$$

$$\Delta G_{R4} = \Delta G_{O_2} - \Delta G_{HOO*} - eU + K_B T \, ln(10) \, pH \qquad (13)$$

In this work, we estimated Gibbs free energy change for reactions (6-9) at pH= 0, T = 298K, and under no applied potential i.e., $U = 0 \, V$ vs. standard hydrogen electrode (SHE). The theoretical OER overpotential which is a metric of OER catalytic activity is defined as-

F*igure 3. Schematic diagram of OER pathway considered in this study. (a) OER at five coordinated Ti (Ti_{cus}) active site and (b) at two coordinated bridge oxygen (O_b) active site. OER at bridge oxygen site is associated with oxygen vacancy creation at bridge site which is shown by the black arrow. The creation of oxygen vacancy releases two extra electrons which eventually reduce two subsurface $Ti-site$ (Ti^{3+}) and form electron polaron as indicated by the green-colored sphere. The oxygen sites which are indicated by 1-4 are the sites where hole polaron formation is considered in this study.*

The theoretical OER overpotential in Volts is then defined as:

$$\eta(V) = {Max(\Delta G_{R_i})}/_e - 1.23\,V \qquad (14)$$

In order to understand hole polaron mediated OER, we examined OER on a clean TiO_2 (110) surface with and without a hole polaron. It is important to note that the presence of a hole polaron represents OER under illuminated conditions, whereas its absence indicates OER under dark conditions. The TiO_2 (110) surface consists of two active sites: five coordinated Ti site (Ti_{cus}) and two coordinated oxygen bridge-site (O_b) (see **Figure 2a**). In this study, we explored OER on both active sites separately, and **Figure 3(a-b)** shows the OER mechanism involving the Ti_{cus} and O_b active site, respectively. We used a clean surface for the OER study because surface Pourbaix diagram indicates that the clean surface is more stable than a *H and *OH covered surface (see **Figure S8**).

For the OER at Ti_{cus} site, the Ti_{cus} site is involved in each step as shown in equation (6-9). However, OER at the O_b active site is initiated with one bridge site oxygen vacancy (shown in **Figure 3b** and **Figure 4**) which is later occupied by OH from H_2O dissociation[34], and the subsequent OER steps are similar to the steps as the Ti_{cus} site. It is important to note that the bridge oxygen vacancy created in the first step releases two extra electrons which eventually form two electron-polarons located at two subsurface Ti atoms then reducing themselves from $Ti^{4+} \rightarrow$ Ti^{3+} (shown in **Figure 4**). The subsurface electron-polaron formation at Ti sites in reduced TiO_2 (110) surface was previously confirmed experimentally[34] as well as theoretically[26,52].

Herein, we also benchmarked previously reported theoretical studies[26,52] of subsurface electron polaron formation at Ti sites in a reduced TiO_2 (110) surface (**Figure 4**). We tried different surface as well as subsurface Ti sites as the electron trapping center. Among all the configurations considered in this study, the lowest energy configuration agrees well with previously reported subsurface electron polaronic structure[26,52]. **Figure 4** shows the lowest energy subsurface electron polaron structure with one bridge oxygen (O_b) vacancy. The details of subsurface electron polaron formation at different surface as well as subsurface Ti atoms are presented in the **Figure S9**. When an *OH molecule attaches to the vacant site, it causes one of the subsurface Ti-sites having +3 oxidation state to oxidize into Ti^{4+} state. On the other hand, when an O* binds to the vacant site, the remaining subsurface Ti^{3+} site undergoes oxidation to become Ti^{4+}. The original arrangement of the two subsurface Ti^{3+} sites is restored when an O_2 molecule leaves the surface in the final step of the OER reaction (see **Figure 3b**).
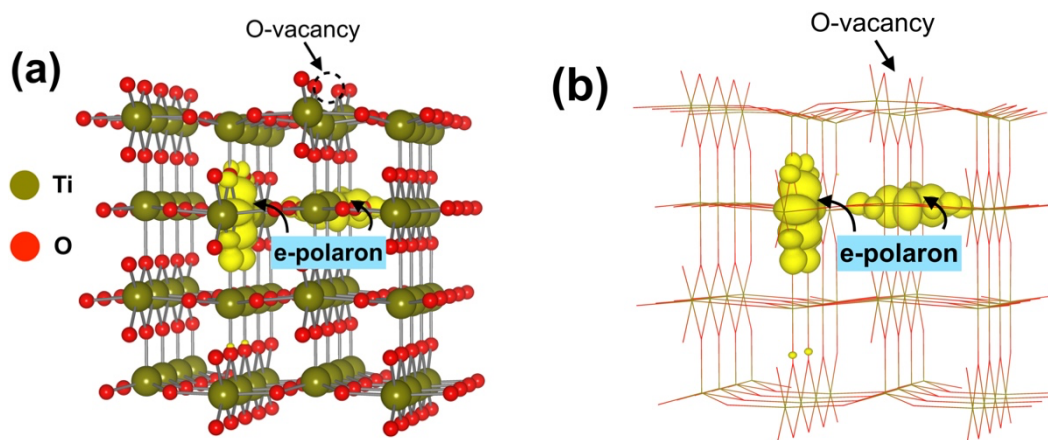
***Figure 4**. Visualization of subsurface electron polaron at Ti-site. (a) Ball and stick model and (b) wire-frame model. The bridge oxygen vacancy on top of the surface is shown as black arrow and*

dotted circle. The yellow iso-surface represents electron polaron at Ti-site and the iso-surface is drawn with an iso-surface value of 0.005 eÅ⁻³.

For an ideal catalyst, the overpotential (η) is defined as zero, which means that $\Delta G_{R1} = \Delta G_{R2} = \Delta G_{R3} = \Delta G_{R4} = 1.23\ eV$. In the present study, we calculated the Gibbs free energy change as well as estimated the OER overpotential considering scenarios with or without hole the polarons on the TiO$_2$ (110) surface. In **Figure-5(a-b),** we present the computed OER free energy landscape for the Ti$_{cus}$ and the O$_b$ sites, respectively. In both scenarios, we established a baseline using a surface devoid of the hole polaron, representing what we term "dark conditions." From this baseline, we charted the free energy curves for the surfaces containing a hole polaron, representing illuminated conditions, at different O-sites (indicated by 1- 4) within the surface as shown in **Figure 3**.

For Ti$_{cus}$ site OER, we stabilized the hole polaron at four distinct positions (marked as 1- 4 in **Figure 3a and 5a**) and calculated the corresponding relative OER free energy. For the O$_b$ site OER, we exclusively stabilized the hole polarons at the surface bridge site in two different locations – one positioned far from the active site and the other in the vicinity of the active site (see **Figures 3b and 5b**). As depicted in **Figure 5(a),** the presence of a hole polaron within the surface enhances the stability of *OH, regardless of its position. Conversely, *O becomes less stable with a surface hole polaron, except when the hole polaron is in an equatorial position. In this case, *O becomes slightly more stable compared to the scenario without a hole polaron. Consequently, the difference in Gibbs free energy $\Delta G_{R2}(= \Delta G_{O*} - \Delta G_{HO*})$ is higher when a surface hole polaron is present, except in the case of an equatorial position. As demonstrated in **Figure 5a,** step R2 emerges as the rate-determining step (RDS) for the Ti$_{cus}$ site- OER. Therefore, all hole polaron configurations, excluding the equatorial one, increase the OER overpotential. Only the equatorial hole polaron reduces the OER overpotential by approximately 4.6% compared to the absence of a hole polaron within the surface.

Analysis of the OER activity at the O$_b$ site. Here, we exclusively focused on hole polarons at the surface bridge site, positioned in two ways – one farther from the active site and the other nearby. In **Figure 5b**, *OH exhibits greater stability regardless of the hole polaron's position. We find that O* becomes more stable when the hole polaron is near the active site but less stable when it is farther away. The situation is the opposite for *OOH, where a hole polaron far from the active site
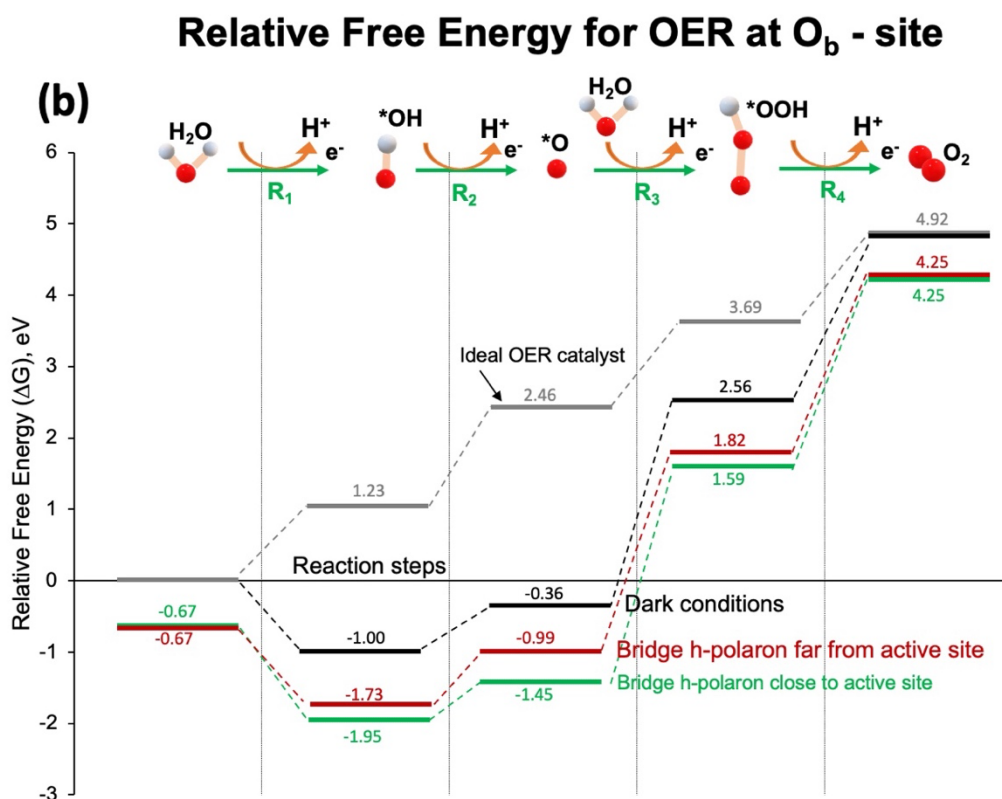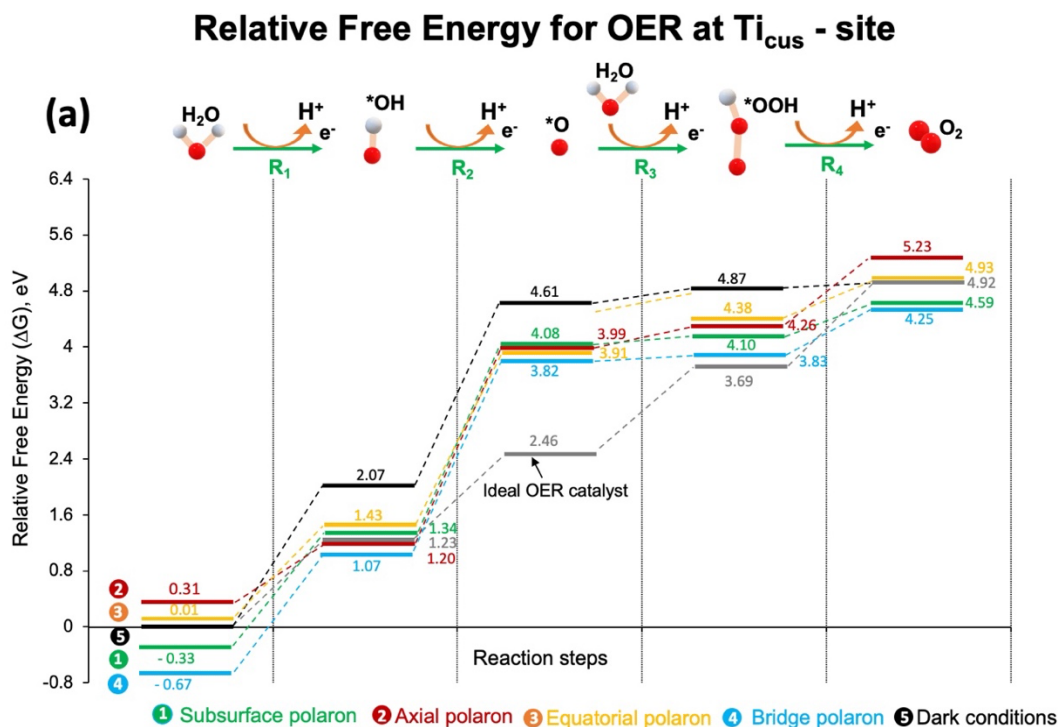
Figure 5. *Diagrams of relative free energy landscapes for OER pathways considered in this study.*
(a) OER at five coordinated Ti (Ti$_{cus}$) active site and (b) OER at two coordinated bridge oxygen

*(O_b) active site. The dashed lines serve as guide only. The calculated reaction energies for OER at both Ti_{cus} and O_b sites are presented in **Table S1** and **Table S2**, respectively.*

enhances stability compared to the scenario without a bridge hole polaron. As depicted in **Figure 5b**, step R3 serves as the rate-determining step (RDS), leading to a reduction in OER overpotential with a hole polaron positioned far from the active site, compared to the absence of a bridge hole polaron. This configuration lowers OER overpotential by approximately 6.5%.

The impact of hole polarons on OER activity is further highlighted in the OER activity plot, shown in **Figure 6a**. This volcano type plot provides a visual representation of the changes in OER onset potential. The plot shows the surface associated with the equatorial polaron has a slight upward shift towards the top of the volcano in the onset potential. This shift signifies that hole polarons at these specific positions effectively decrease the OER overpotential. Indeed, these configurations lead to a reduction in OER overpotential by approximately 0.06 and 0.12 eV (4.6-6.5)% compared to the scenario without the hole polarons as illustrated in **Figures 6b,c**.
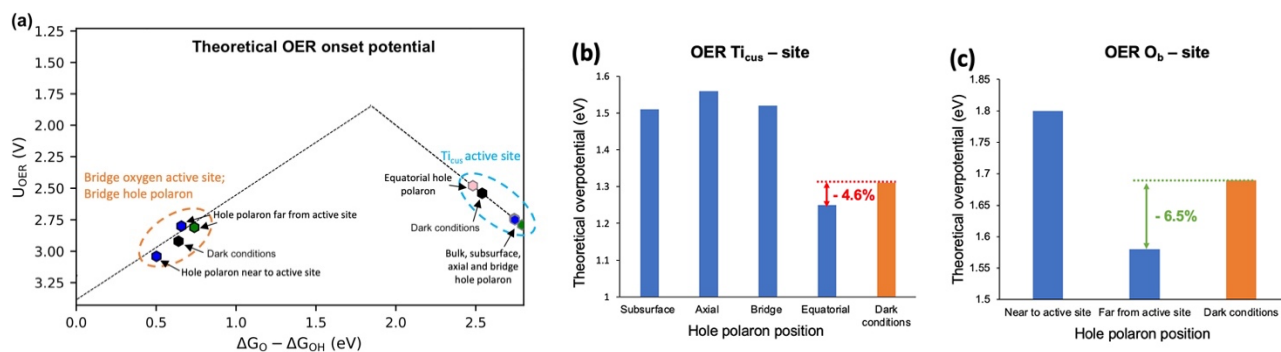
Figure 6. OER activity plots. (a) Volcano plot for OER onset potential. The left-hand side leg corresponds to O_b site OER and right-hand side leg corresponds to Ti_{cus} site OER. (b) OER overpotential for Ti_{cus} site OER and (c) OER overpotential for O_b site OER. In both cases, dark conditions (without hole polaron) overpotential was considered as a reference.

CONCLUSIONS

In this study, we applied DFT+U theory fitted to hybrid DFT to conduct a comprehensive simulations of surface polaron formation and describe the complex polaronic OER mechanism on a rutile TiO_2 (110) surface. We identify the thermodynamic stability of hole polarons at various oxygen sites, particularly emphasizing their propensity for bulk, bridge and subsurface oxygen

localization. Obtained polaronic energy levels revealed deep defect levels for most configurations within the bandgap, while axial and equatorial hole polarons exhibited shallower behavior. These hole polarons were demonstrated to stabilize *OH and *O species on the surface, albeit with varied impacts on the OER overpotential. Notably, two configurations showcased reduced overpotential in comparison to non-polaronic conditions. Hole polaron at equatorial (for Ti_{cus} site OER) and far away bridge site (for O_b site OER) observes approximately (4.6 – 6.5) % OER overpotential reduction. We have also shown that equatorial polaron has a shallow location near the VBM which can be easily ionized for use in OER. Surface bridge oxygen site in the OER mechanism involves subsurface electron polaron formation at Ti site during turnover. Although this study did not yield significant OER enhancement, it offers important insights into polaronic OER within transition metal oxides and related metal chalcogenides. This work underscores the pivotal role of polarons in carrier separation and catalytic activity, holding promise for advancing PEC H_2O splitting technology and contributing to a carbon-free, green energy economy in the 21st century.

ACKNOWLEDGEMENT

COMPETING FINANCIAL INTEREST

The authors declare no competing conflicts of interests, financial or otherwise.

DATA AVAILABILITY

All atomic configurations and DFT calculated energies are available in CatalysisHub[60] under https://www.catalysis-hub.org/publications/Sarker Prediction2023.

REFERENCES

[1] M. Grätzel, "Photoelectrochemical cells," Nature **414**(6861), 338–344 (2001).
[2] T. Kunene, L. Xiong, and J. Rosenthal, "Solar-powered synthesis of hydrocarbons from carbon dioxide and water," Proc. Natl. Acad. Sci. U.S.A. **116**(20), 9693–9695 (2019).

[3] M. Rahaman, V. Andrei, D. Wright, E. Lam, C. Pornrungroj, S. Bhattacharjee, C.M. Pichler, H.F. Greer, J.J. Baumberg, and E. Reisner, "Solar-driven liquid multi-carbon fuel production using a standalone perovskite–BiVO4 artificial leaf," Nat Energy **8**(6), 629–638 (2023).

[4] V. Balzani, G. Pacchioni, M. Prato, and A. Zecchina, "Solar-driven chemistry: towards new catalytic solutions for a sustainable world," Rend. Fis. Acc. Lincei **30**(3), 443–452 (2019).

[5] N.S. Lewis, "Research opportunities to advance solar energy utilization," Science **351**(6271), aad1920 (2016).

[6] A.A. Peterson, F. Abild-Pedersen, F. Studt, J. Rossmeisl, and J.K. Nørskov, "How copper catalyzes the electroreduction of carbon dioxide into hydrocarbon fuels," Energy Environ. Sci. **3**(9), 1311 (2010).

[7] K.P. Kuhl, T. Hatsukade, E.R. Cave, D.N. Abram, J. Kibsgaard, and T.F. Jaramillo, "Electrocatalytic Conversion of Carbon Dioxide to Methane and Methanol on Transition Metal Surfaces," J. Am. Chem. Soc. **136**(40), 14107–14113 (2014).

[8] C.W. Li, J. Ciston, and M.W. Kanan, "Electroreduction of carbon monoxide to liquid fuel on oxide-derived nanocrystalline copper," Nature **508**(7497), 504–507 (2014).

[9] A. Kudo, and Y. Miseki, "Heterogeneous photocatalyst materials for water splitting," Chem. Soc. Rev. **38**(1), 253–278 (2009).

[10] A. Walsh, K.-S. Ahn, S. Shet, M.N. Huda, T.G. Deutsch, H. Wang, J.A. Turner, S.-H. Wei, Y. Yan, and M.M. Al-Jassim, "Ternary cobalt spinel oxides for solar driven hydrogen production: Theory and experiment," Energy Environ. Sci. **2**(7), 774 (2009).

[11] A. Fujishima, and K. Honda, "Electrochemical Photolysis of Water at a Semiconductor Electrode," Nature **238**(5358), 37–38 (1972).

[12] T.L. Thompson, and J.T. Yates, "Surface Science Studies of the Photoactivation of TiO $_2$ New Photochemical Processes," Chem. Rev. **106**(10), 4428–4453 (2006).

[13] A.J. Nozik, "Photoelectrolysis of water using semiconducting TiO2 crystals," Nature **257**(5525), 383–386 (1975).

[14] I.C. Man, H. Su, F. Calle-Vallejo, H.A. Hansen, J.I. Martínez, N.G. Inoglu, J. Kitchin, T.F. Jaramillo, J.K. Nørskov, and J. Rossmeisl, "Universality in Oxygen Evolution Electrocatalysis on Oxide Surfaces," ChemCatChem **3**(7), 1159–1165 (2011).

[15] S. Lany, "Semiconducting transition metal oxides," J. Phys.: Condens. Matter **27**(28), 283203 (2015).

[16] Z. Yin, M. Tordjman, Y. Lee, A. Vardi, R. Kalish, and J.A. Del Alamo, "Enhanced transport in transistor by tuning transition-metal oxide electronic states interfaced with diamond," Sci. Adv. **4**(9), eaau0480 (2018).

[17] M. Setvin, C. Franchini, X. Hao, M. Schmid, A. Janotti, M. Kaltak, C.G. Van De Walle, G. Kresse, and U. Diebold, "Direct View at Excess Electrons in TiO $_2$ Rutile and Anatase," Phys. Rev. Lett. **113**(8), 086402 (2014).

[18] S.X. Zhang, D.C. Kundaliya, W. Yu, S. Dhar, S.Y. Young, L.G. Salamanca-Riba, S.B. Ogale, R.D. Vispute, and T. Venkatesan, "Niobium doped TiO2: Intrinsic transparent metallic anatase versus highly resistive rutile phase," Journal of Applied Physics **102**(1), 013701 (2007).

[19] Y. Obara, H. Ito, T. Ito, N. Kurahashi, S. Thürmer, H. Tanaka, T. Katayama, T. Togashi, S. Owada, Y. Yamamoto, S. Karashima, J. Nishitani, M. Yabashi, T. Suzuki, and K. Misawa, "Femtosecond time-resolved X-ray absorption spectroscopy of anatase TiO2 nanoparticles using XFEL," Structural Dynamics **4**(4), 044033 (2017).

[20] S. Yang, A.T. Brant, N.C. Giles, and L.E. Halliburton, "Intrinsic small polarons in rutile TiO $_2$," Phys. Rev. B **87**(12), 125201 (2013).

[21] P. Krüger, S. Bourgeois, B. Domenichini, H. Magnan, D. Chandesris, P. Le Fèvre, A.M. Flank, J. Jupille, L. Floreano, A. Cossaro, A. Verdini, and A. Morgante, "Defect States at the TiO $_2$ (110) Surface Probed by Resonant Photoelectron Diffraction," Phys. Rev. Lett. **100**(5), 055501 (2008).

[22] S. Moser, L. Moreschini, J. Jaćimović, O.S. Barišić, H. Berger, A. Magrez, Y.J. Chang, K.S. Kim, A. Bostwick, E. Rotenberg, L. Forró, and M. Grioni, "Tunable Polaronic Conduction in Anatase TiO $_2$," Phys. Rev. Lett. **110**(19), 196403 (2013).

[23] M. Reticcioli, M. Setvin, M. Schmid, U. Diebold, and C. Franchini, "Formation and dynamics of small polarons on the rutile TiO 2 (110) surface," Phys. Rev. B **98**(4), 045306 (2018).

[24] S. Selcuk, and A. Selloni, "Facet-dependent trapping and dynamics of excess electrons at anatase TiO2 surfaces and aqueous interfaces," Nature Mater **15**(10), 1107–1112 (2016).

[25] E. Pastor, M. Sachs, S. Selim, J.R. Durrant, A.A. Bakulin, and A. Walsh, "Electronic defects in metal oxide photocatalysts," Nat Rev Mater **7**(7), 503–521 (2022).

[26] A.C. Papageorgiou, N.S. Beglitis, C.L. Pang, G. Teobaldi, G. Cabailh, Q. Chen, A.J. Fisher, W.A. Hofer, and G. Thornton, "Electron traps and their effect on the surface chemistry of TiO 2 (110)," Proc. Natl. Acad. Sci. U.S.A. **107**(6), 2391–2396 (2010).

[27] P. Gono, J. Wiktor, F. Ambrosio, and A. Pasquarello, "Surface Polarons Reducing Overpotentials in the Oxygen Evolution Reaction," ACS Catal. **8**(7), 5847–5851 (2018).

[28] C. Franchini, M. Reticcioli, M. Setvin, and U. Diebold, "Polarons in materials," Nat Rev Mater **6**(7), 560–586 (2021).

[29] N.A. Deskins, R. Rousseau, and M. Dupuis, "Localized Electronic States from Surface Hydroxyls and Polarons in TiO 2 (110)," J. Phys. Chem. C **113**(33), 14583–14586 (2009).

[30] N.A. Deskins, and M. Dupuis, "Intrinsic Hole Migration Rates in TiO 2 from Density Functional Theory," J. Phys. Chem. C **113**(1), 346–358 (2009).

[31] N.A. Deskins, and M. Dupuis, "Electron transport via polaron hopping in bulk Ti O 2 : A density functional theory characterization," Phys. Rev. B **75**(19), 195212 (2007).

[32] J.R. De Lile, A. Bahadoran, S. Zhou, and J. Zhang, "Polaron in TiO 2 from First-Principles: A Review," Advcd Theory and Sims **5**(2), 2100244 (2022).

[33] L.M. Carneiro, S.K. Cushing, C. Liu, Y. Su, P. Yang, A.P. Alivisatos, and S.R. Leone, "Excitation-wavelength-dependent small polaron trapping of photoexcited carriers in α-Fe2O3," Nature Mater **16**(8), 819–825 (2017).

[34] Z. Zhang, O. Bondarchuk, B.D. Kay, J.M. White, and Z. Dohnálek, "Imaging Water Dissociation on TiO 2 (110): Evidence for Inequivalent Geminate OH Groups," J. Phys. Chem. B **110**(43), 21840–21845 (2006).

[35] C. Cheng, Y. Zhu, W.-H. Fang, R. Long, and O.V. Prezhdo, "CO Adsorbate Promotes Polaron Photoactivity on the Reduced Rutile TiO 2 (110) Surface," JACS Au **2**(1), 234–245 (2022).

[36] B. Guzelturk, T. Winkler, T.W.J. Van De Goor, M.D. Smith, S.A. Bourelle, S. Feldmann, M. Trigo, S.W. Teitelbaum, H.-G. Steinrück, G.A. De La Pena, R. Alonso-Mori, D. Zhu, T. Sato, H.I. Karunadasa, M.F. Toney, F. Deschler, and A.M. Lindenberg, "Visualization of dynamic polaronic strain fields in hybrid lead halide perovskites," Nat. Mater. **20**(5), 618–623 (2021).

[37] C. Lohaus, A. Klein, and W. Jaegermann, "Limitation of Fermi level shifts by polaron defect states in hematite photoelectrodes," Nat Commun **9**(1), 4309 (2018).

[38] J. Wiktor, F. Ambrosio, and A. Pasquarello, "Role of Polarons in Water Splitting: The Case of BiVO 4," ACS Energy Lett. **3**(7), 1693–1697 (2018).

[39] A.J.E. Rettie, W.D. Chemelewski, J. Lindemuth, J.S. McCloy, L.G. Marshall, J. Zhou, D. Emin, and C.B. Mullins, "Anisotropic small-polaron hopping in W:BiVO4 single crystals," Applied Physics Letters **106**(2), 022106 (2015).

[40] G. Kresse, and J. Furthmüller, "Efficiency of ab-initio total energy calculations for metals and semiconductors using a plane-wave basis set," Computational Materials Science **6**(1), 15–50 (1996).

[41] A. Hjorth Larsen, J. Jørgen Mortensen, J. Blomqvist, I.E. Castelli, R. Christensen, M. Dułak, J. Friis, M.N. Groves, B. Hammer, C. Hargus, E.D. Hermes, P.C. Jennings, P. Bjerre Jensen, J. Kermode, J.R. Kitchin, E. Leonhard Kolsbjerg, J. Kubal, K. Kaasbjerg, S. Lysgaard, J. Bergmann Maronsson, T. Maxson, T. Olsen, L. Pastewka, A. Peterson, C. Rostgaard, J. Schiøtz, O. Schütt, M. Strange, K.S. Thygesen, T. Vegge, L. Vilhelmsen, M. Walter, Z. Zeng, and K.W. Jacobsen, "The atomic simulation environment—a Python library for working with atoms," J. Phys.: Condens. Matter **29**(27), 273002 (2017).

[42] J.P. Perdew, and Y. Wang, "Accurate and simple analytic representation of the electron-gas correlation energy," Phys. Rev. B **45**(23), 13244–13249 (1992).

[43] P.E. Blöchl, "Projector augmented-wave method," Phys. Rev. B **50**(24), 17953–17979 (1994).

[44] V.I. Anisimov, J. Zaanen, and O.K. Andersen, "Band theory and Mott insulators: Hubbard U instead of Stoner I," Phys. Rev. B **44**(3), 943–954 (1991).

[45] A.I. Liechtenstein, V.I. Anisimov, and J. Zaanen, "Density-functional theory and strong interactions: Orbital ordering in Mott-Hubbard insulators," Phys. Rev. B **52**(8), R5467–R5470 (1995).

[46] S.L. Dudarev, G.A. Botton, S.Y. Savrasov, C.J. Humphreys, and A.P. Sutton, "Electron-energy-loss spectra and the structural stability of nickel oxide: An LSDA+U study," Phys. Rev. B **57**(3), 1505–1509 (1998).

[47] J. Heyd, G.E. Scuseria, and M. Ernzerhof, "Hybrid functionals based on a screened Coulomb potential," The Journal of Chemical Physics **118**(18), 8207–8215 (2003).

[48] B.J. Morgan, and G.W. Watson, "A DFT+U description of oxygen vacancies at the TiO2 rutile (110) surface," Surface Science **601**(21), 5034–5041 (2007).

[49] V. Pasumarthi, T. Liu, M. Dupuis, and C. Li, "Charge carrier transport dynamics in W/Mo-doped BiVO$_4$: first principles-based mesoscale characterization," J. Mater. Chem. A **7**(7), 3054–3065 (2019).

[50] T. Liu, X. Zhou, M. Dupuis, and C. Li, "The nature of photogenerated charge separation among different crystal facets of BiVO$_4$ studied by density functional theory," Phys. Chem. Chem. Phys. **17**(36), 23503–23510 (2015).

[51] C.J. Calzado, N.C. Hernández, and J.Fdez. Sanz, "Effect of on-site Coulomb repulsion term U on the band-gap states of the reduced rutile (110) Ti O 2 surface," Phys. Rev. B **77**(4), 045118 (2008).

[52] S. Chrétien, and H. Metiu, "Electronic Structure of Partially Reduced Rutile TiO$_2$ (110) Surface: Where Are the Unpaired Electrons Located?," J. Phys. Chem. C **115**(11), 4696–4705 (2011).

[53] U. Diebold, "The surface science of titanium dioxide," Surface Science Reports **48**(5–8), 53–229 (2003).

[54] H. Sezen, M. Buchholz, A. Nefedov, C. Natzeck, S. Heissler, C. Di Valentin, and C. Wöll, "Probing electrons in TiO2 polaronic trap states by IR-absorption: Evidence for the existence of hydrogenic states," Sci Rep **4**(1), 3808 (2014).

[55] H.L. Tuller, and S.R. Bishop, "Point Defects in Oxides: Tailoring Materials Through Defect Engineering," Annu. Rev. Mater. Res. **41**(1), 369–398 (2011).

[56] J.S. Park, S. Kim, Z. Xie, and A. Walsh, "Point defect engineering in thin-film solar cells," Nat Rev Mater **3**(7), 194–210 (2018).

[57] A.R. Elmaslmane, M.B. Watkins, and K.P. McKenna, "First-Principles Modeling of Polaron Formation in TiO$_2$ Polymorphs," J. Chem. Theory Comput. **14**(7), 3740–3751 (2018).

[58] F. Oba, and Y. Kumagai, "Design and exploration of semiconductors from first principles: A review of recent advances," Appl. Phys. Express **11**(6), 060101 (2018).

[59] J. Rossmeisl, Z.-W. Qu, H. Zhu, G.-J. Kroes, and J.K. Nørskov, "Electrolysis of water on oxide surfaces," Journal of Electroanalytical Chemistry **607**(1–2), 83–89 (2007).

[60] K.T. Winther, M.J. Hoffmann, J.R. Boes, O. Mamun, M. Bajdich, and T. Bligaard, "Catalysis-Hub.org, an open electronic structure database for surface reactions," Sci Data **6**(1), 75 (2019).